Time-resolved Temperature Inferences Utilizing the TiO $A^3\Phi \rightarrow X^3\Delta$ Band in Laser-induced Plasma

ALEXANDER C. WOODS[1], CHRISTIAN G. PARIGGER,[1,a] AND JAMES O. HORNKOHL[2]

[1]*University of Tennessee Space Institute, Center for Laser Applications, Tullahoma, TN 37388, USA*
[2]*Hornkohl Consulting, Tullahoma, TN, 37388, USA*
[a]*Corresponding author: cparigge@tennessee.edu*

ABSTRACT: Current efforts involving laser-induced breakdown spectroscopy investigate titanium monoxide (TiO) transitions, inferring temperature for various delay times following laser-induced breakdown. A titanium sample resting in laboratory air is repeatedly exposed to nanosecond pulsed radiation generated by a Nd:YAG laser. Spectral measurements are collected at various delay times ranging from 20 - 95 μs subsequent to the laser event. Temperature inferences at select time delays times are facilitated by fitting synthetic spectra of varying micro-plasma parameters to the gathered spectra utilizing a Nelder-Mead algorithm. In some instances, these inferences provide a temperature versus time profile containing a local minimum, as an increase in the inferred temperature begins at later delay times. This phenomenon, possibly due to combustion, is investigated by analyzing signal to noise ratios with respect to their effect on the inferred temperature of diatomic molecular transitions. Temperature inferences resulting by fitting only regions of the measured spectra believed to be dominated by rotational or vibrational diatomic molecular transitions provide insight into the temporal evolution of the TiO $A^3\Phi \rightarrow X^3\Delta$, $\Delta v = 0$ molecular transitions in the laser-induced plasma.

PACS numbers: 52.50.Jm, 33.20.-t, 78.47.dc, 82.80.-d, 95.55Qf, 95.75.Fg, 81.15.-z.

Keywords: laser-induced breakdown spectroscopy; molecular spectroscopy, time- resolved spectroscopy, laser-induced breakdown, spectroscopy in astronomy, thin film deposition and fabrication.

I. INTRODUCTION

Titanium monoxide (TiO) has been traditionally studied in astrophysical contexts and is the focus of current astrophysical research[1–4]. The presence of TiO molecular spectra serves as a means of classifying K and M type stars, as TiO is a major contributor to the spectroscopic features of K and M type stars ranging from the visible to the infrared. While the TiO transitions become less prominent with decreasing temperature, they may still be observed well into the L domain and hence play a role in the classification of L type dwarfs, as well[5]. It is the weakening of TiO lines in the optical region for L type dwarfs which allows for hydride bands and monatomic alkali lines to become more prominent[6]. Subsequently, the effect of TiO in stellar atmospheres is an important topic of research. Investigations into the radiative opacity of TiO in stellar atmospheres reveals relations between opacity and temperature[7,8]. Both theoretical and observational efforts have been focused on TiO opacity and its relation to temperature[9,10]. This has allowed for advances in the modeling of stellar atmospheres[11].

The behavior of TiO in laser-induced plasma is another research area of interest. Among its various applications in paints and sunscreens, TiO_2 is also a suitable molecule for thin film applications. Due to its photocatalytic properties[12], TiO_2 thin films may be used for water and air purification and treatment[13], and they are a possible candidate for solar cell applications[14,15]. As a popular technique for producing thin films, pulsed laser deposition (PLD) utilizes laser ablation to provide material for the thin film. In a titanium containing laser-induced plasma, the TiO molecule is a precursor to TiO_2. Thus, the evolution of the temperature of TiO in a laser-induced plasma is of fundamental importance concerning the use of titanium in PLD[16].

The focus of this effort includes fitting computed spectra to experimental spectra gathered at various delay times following laser-induced breakdown (LIB). Computing synthetic spectra for diatomic molecules is dependent upon line strength files. The process of computing line strength files requires potential energy curves for the upper and lower levels of a transition. Hönl-London factors may then be calculated and implemented as a selection rule, where non-zero Hönl-London values represent an allowed transition. For these transitions, Franck-Condon factors and r-centroids are calculated and included in a Taylor's series expansion of the electronic transition moment. Brief discussions including specifics of the computations of the TiO line strength files used in this research are found in Parigger *et al.* 2012[17] and Woods *et al.* 2012[18].
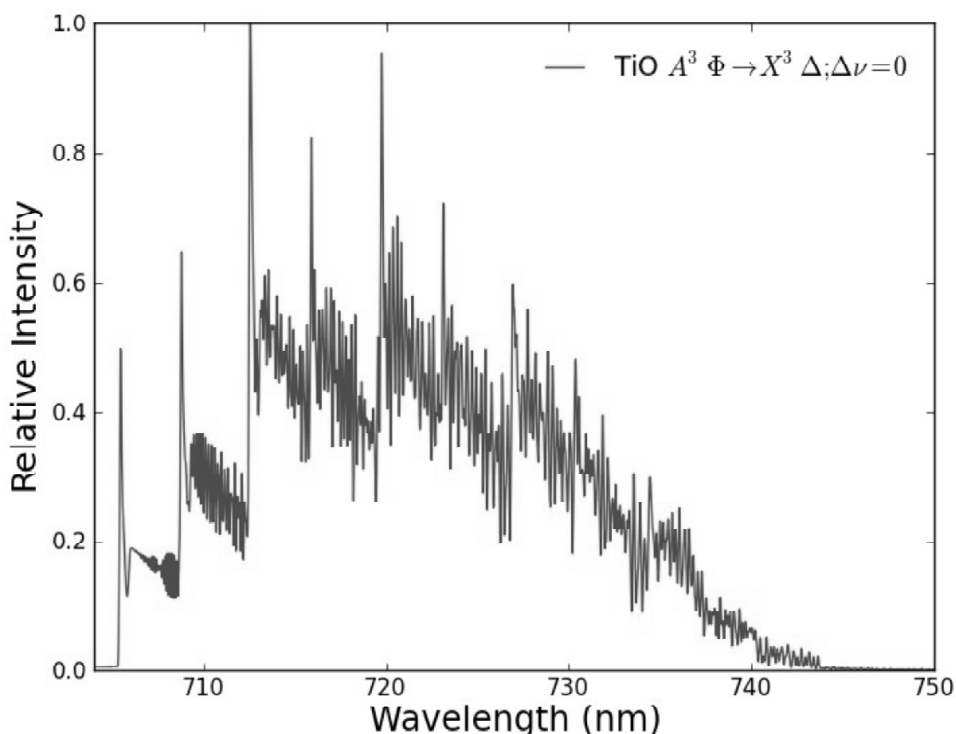
Figure 1: Computed spectra for the TiO $A^3\Phi \rightarrow X^3\Delta$, $\Delta v = 0$ transition band, corresponding to a temperature of T = 4000 K and resolution FWHM = 0.1 nm.

The line strength file allows for a specific spectrum to be represented given various parameters such as spectral resolution, peak intensity, baseline offset, a linear, quadratic, or cubic baseline, and temperature. For this experiment, a Nelder Mead algorithm is implemented to fit the synthetic spectra to experimentally obtained spectra. The Nelder Mead method provides a multi-parameter fit, which allows for inferences to be made by determining the parameter values resulting in the best fitting model. For the purposes of this research, the fitting algorithm is used primarily to infer temperature of the TiO γ, $A^3\Phi \rightarrow X^3\Delta$, transition. Figure 1 illustrates a synthetic spectrum utilizing the computed line strength files at the University of Tennessee Space Institute.

The accuracy of temperature inferences made by diatomic spectrum fitting is subject to the ability to isolate the transitions of interest amongst a measured spectrum. The ratios of peak to peak intensities of certain spectral transitions for diatomic molecules are temperature dependent. Increased contributions to what is considered to be the spectral background to the diatomic transitions may distort such ratios and thus temperature inferences. This communication reports investigations specific to the TiO $A^3\Phi \rightarrow X^3\Delta$, $\Delta v = 0$ band in the $705 - 715$ nm spectral range. This particular transition band is advantageous for the purposes of temperature inferences by diatomic spectrum fitting because there are minimal contributions attributed to atomic lines and other TiO molecular transitions in the spectral region[18].

II. EXPERIMENT

Our experimental setup utilized a typical laser-induced breakdown spectroscopy (LIBS) design. An illustration of the experimental schematic used for collecting data is presented elsewhere[19]. A 13 ns Q-switched Nd: YAG Quanta-Ray DCR-2A(10) laser provided 160 mJ per pulse to the surface of a Ti 6-4 sample. A Jobin Yvon HR 640 spectrometer equipped with a 1800 grooves/mm grating and an intensified linear diode array (model 1460 Princeton Applied Research detector/controller optical multichannel analyzer) was implemented as a means of gated detection. The laser beam is focused to approximately a 1 mm spot size vertically downward onto the Ti sample. The experiment is conducted in an open air environment, allowing the oxygen to be provided by the ambient laboratory air. The ablation plume is imaged onto the spectrometer's slit by two field lenses, which are chosen to match the $f^{\#}$ of the spectrometer. A low-pass filter at 400 nm is positioned between the lenses, eliminating second order Ti atomic lines from the measurement.

A wave generator is used as a means to trigger the laser as well as the CCD and optical multichannel analyzer. The laser is triggered at 10 Hz, while the detection devices are triggered at 50 Hz. Only measurements corresponding to a laser event are collected as data. The other four measurements are ignored and serve to wash the detection devices of persistent electronic features from the previous laser event. The spectra to be used for the temperature analysis are each comprised of 100 individual measurements. The output of a Si biased detector, used to measure the laser pulse, and the pulse generator, used to trigger and gate the CCD, are observed using an oscilloscope. A delay generator is then utilized to ensure the signals are synchronous at the laser event, which is chosen to be the initial time, $t_{delay} = 0$.

Measurements observing the TiO γ, $\Delta v = 0$ transition band were collected at time delays ranging from 20 to 60 μs with a gate width of 5 μs. These measurements were gathered by incrementally increasing the time delay with 5 μs intervals. Then, another set of measurements were collected at time delays ranging from 26 to 60 μs with a 2 μs gate width measured at 2 μs intervals. A third experimental run gathered measurements of the γ bands at delay times ranging from 26 to 86 μs with a 2 μs gate width at intervals of 4 μs. For the third experimental run a different Ti slab, which had not previously experienced laser ablation, was used to produce the plasma. Two additional measurements were also taken with this Ti sample at 90 μs and 95 μs time delays using a 2 μs gate width.

III. RESULTS

Figures 2-3 demonstrate the results of fitting computed spectra to a measured spectrum. A typical inferred temperature results from the fitting of computed spectra to a measured spectrum over the full wavelength range of the measurement. For this investigation, spectral regions consisting of predominantly rotational or vibrational structure are fit individually, as well. Figure 2 presents a measured spectrum along with the computed spectra used to infer temperature. Figure 3 illustrates the results of fitting the same measurement with only the predominantly rotational and vibrational regions of the computed synthetic spectra, respectively. The synthetic spectra used to infer temperature represents the TiO $A^3\Phi \rightarrow X^3\Delta$, $\Delta v = 0$ band. The measured data shown corresponds to a time delay of 95 μs collected using a 2 μs window.

This particular measurement is noteworthy because it is observed that, for the third experimental run, the TiO spectra at the latest measurement times had less background contributions than at earlier time delays. This can be expected due to the overall decrease in signal with increasing time after optical breakdown. However, previous investigations concerning TiO in laser ablation plumes sometimes contain the presence of Ti atomic lines persisting at relatively long time delays[17,18]. As time delay further increases, diatomic spectra become less prominent and ultimately vanish. The measurements gathered for this region of the $A^3\Phi \rightarrow X^3\Delta$ band show minimal contributions from atomic spectral lines, and the TiO contributions remain discernable even at time delays such as this.

Tables 1-3 present the inferred temperatures of the TiO $A^3\Delta \rightarrow X^3\Delta$, $\Delta v = 0$ system resulting from the Nelder-Mead fitting routine at various delay times following laser-induced breakdown. The first column of temperature values, labeled "T(K)", represents the temperature inferred by fitting the entire range of the measured spectrum with our computed spectra. The temperature values falling under columns labeled "Rotational T(K)" and "Vibrational
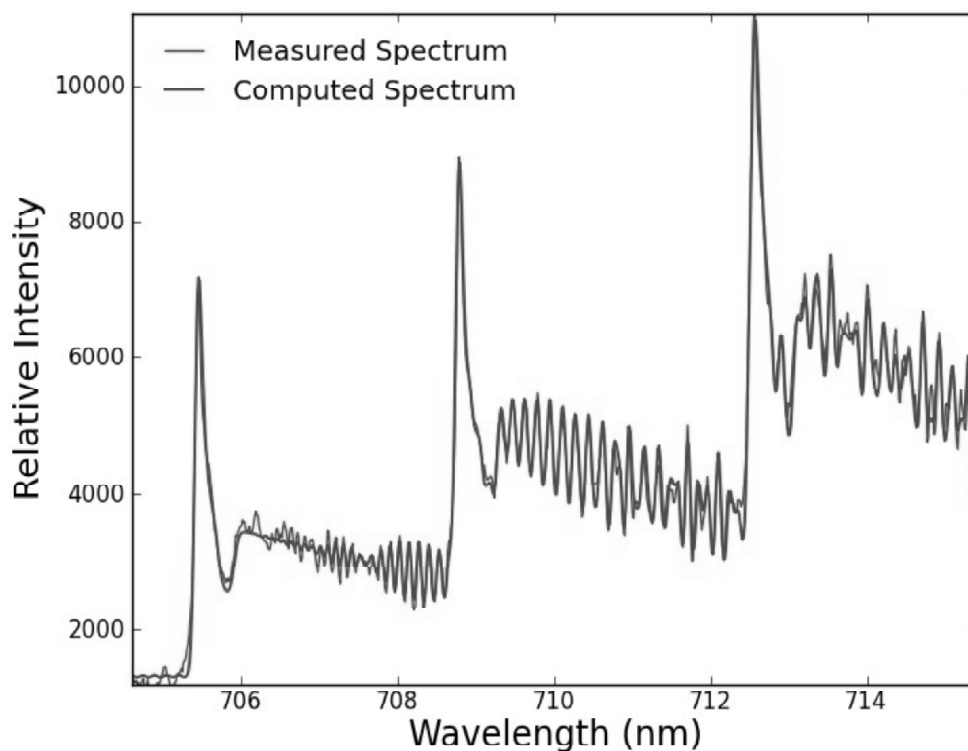
**Figure 2: TiO $A^3\Phi \to X^3\Delta$ transition collected at a time delay t_{delay} = 95 μs with a 2 μs gate width.
The fit results in an inferred temperature of 3335 K.**
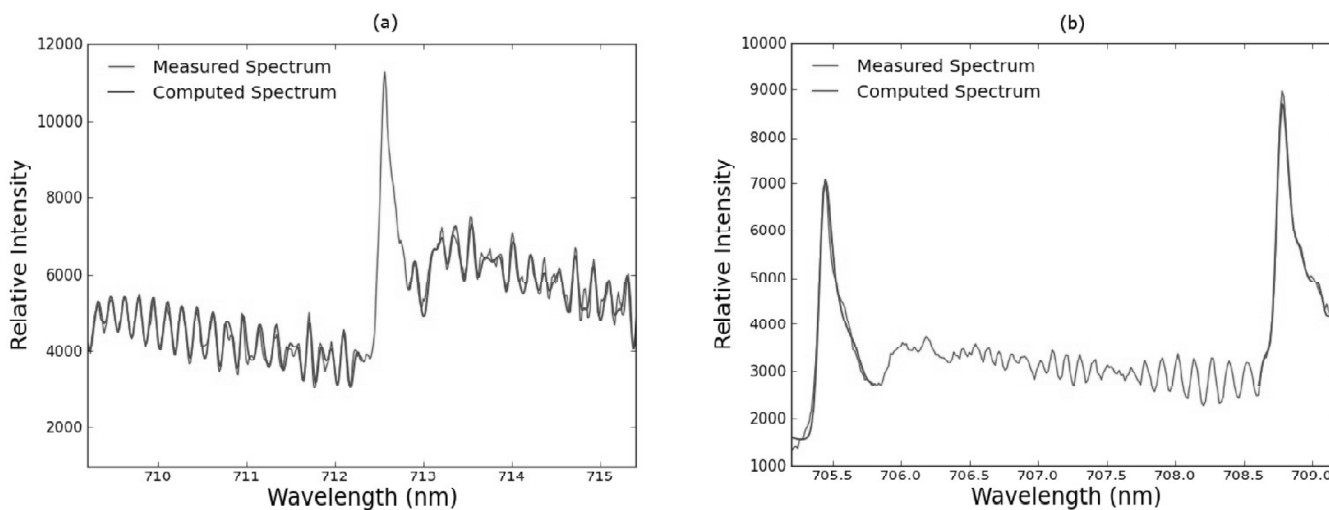
Figure 3: TiO $A^3\Phi \to X^3\Delta$ transition collected at a time delay t_{delay} = 95 μs with a 2 μs gate width.
(a) **The fit of the rotational structure results in an inferred temperature of 3216 K.**
(b) **The fit of the vibrational structure results in an inferred temperature of 4178 K.**

T(K)" represent the inferred temperatures by analyzing only the region containing predominantly rotational and vibrational structure, respectively.

Figures 4-6 provide visual representations of Tables I–III, respectively. Figure 4 illustrates that inferred temperatures listed in Table 1 contain a local minimum between 20 and 60 μs subsequent to laser-induced breakdown. The second experimental run presented in Fig. 5 provides a more resolved glimpse, with respect to time delay, at a spectral region where the first experimental run implies temperature decreasing to a local minimum. In contrast,

Table I

The table displays the inferred TiO temperatures for the $A^3\Phi \rightarrow X^3\Delta$ transition at various time delays. Each measurement was collected using a 5 μs gate width. The rotational and vibrational temperatures were obtained by fitting portions of the spectra containing only rotational and vibrational transitions, respectively. An asterisk indicates that the signal to noise ratio of the measured spectrum is insufficient for a reasonable temperature inference.

$t_{delay}(\mu s)$	T(K)	Rotational T(K)	Vibrational T(K)
60	4269	5332	3598
55	3802	3874	3081
50	3437	3196	2682
45	3140	2894	2435
40	3026	2642	2519
35	3075	2660	2721
30	3189	3009	3140
25	3339	3308	4226
20	3985	5054	*

Table II

The table displays the inferred TiO temperatures for the $A^3\Phi \rightarrow X^3\Delta$ transition at various time delays. Each measurement was collected using a 2 μs gate width. The rotational and vibrational temperatures were obtained by fitting portions of the spectra containing only rotational and vibrational transitions, respectively.

$t_{delay}(\mu s)$	T(K)	Rotational T(K)	Vibrational T(K)
26	3459	3742	5831
28	3401	3505	4823
30	3438	3830	3956
32	3404	3394	3312
34	3297	3091	3055
36	3309	3101	3191

Table III

The table displays the inferred TiO temperatures for the $A^3\Phi \rightarrow X^3\Delta$ transition at various time delays. Each measurement was collected using a 2 μs gate width. The rotational and vibrational temperatures were obtained by fitting portions of the spectra containing only rotational and vibrational transitions, respectively.

$t_{delay}(\mu s)$	T(K)	Rotational T(K)	Vibrational T(K)
26	4652	4049	3946
30	4401	3767	3347
34	4747	3718	3438
38	4344	3556	3146
42	4661	3733	3725
46	4349	4023	3203
50	3978	3577	4910
54	3618	3099	3944
58	3547	3012	5467
62	3546	3048	5013
66	3756	3206	5540
70	3219	3116	4386
74	3178	2908	4684
78	3309	3031	4312
82	3405	3183	4226
86	3421	3185	5633
90	3665	3376	5407
95	3335	3216	4178

Figure 6 characterizes the inferred temperature versus time delay over the broader range between 26 and 95 μs. Utilizing a different Ti sample than the first two experimental runs, a local minimum in temperature is not apparent in the third experimental run.
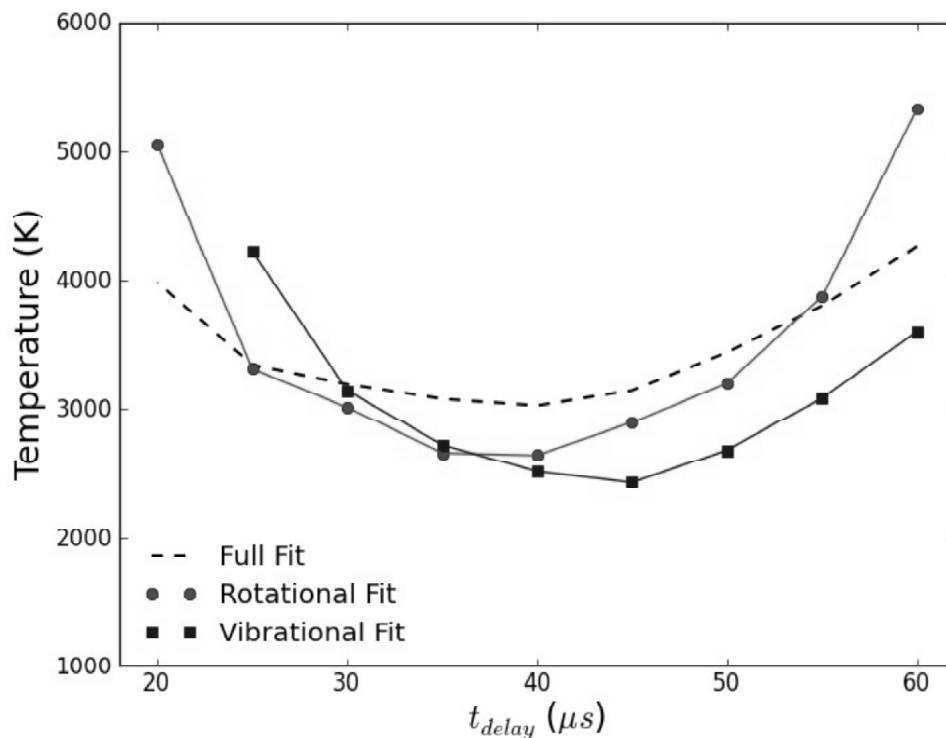
Figure 4: Inferred temperatures from Table 1 for the TiO $A^3 \Phi \rightarrow X^3 \Delta$ transition collected at various time delays
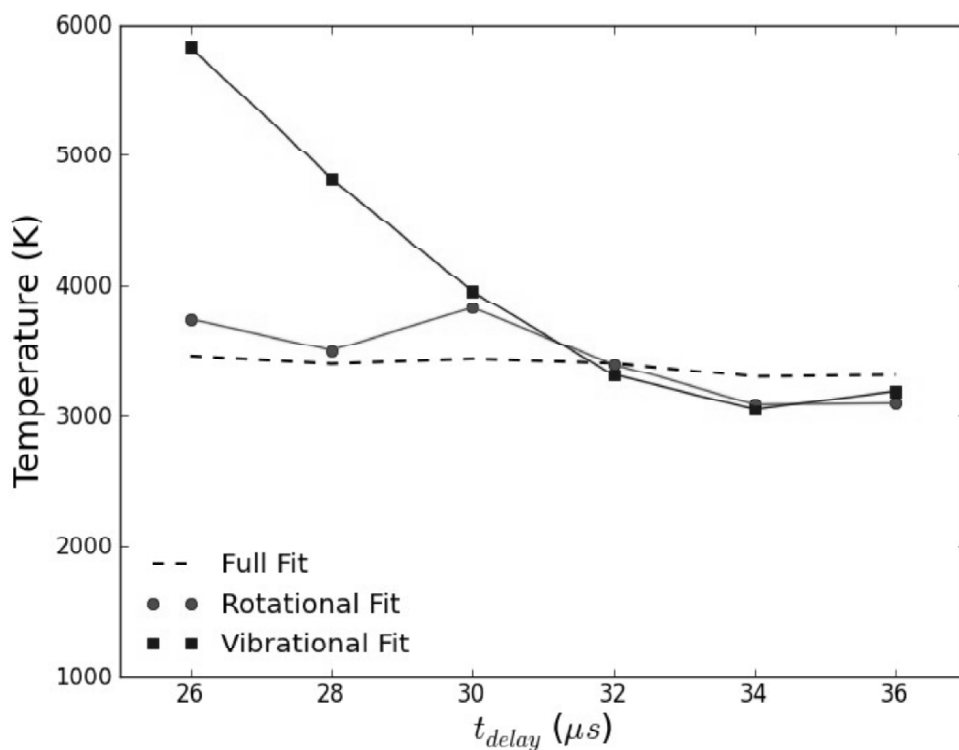
Figure 5: Inferred temperatures from Table 2 for the TiO $A^3 \Phi \rightarrow X^3 \Delta$ transition collected at various time delays
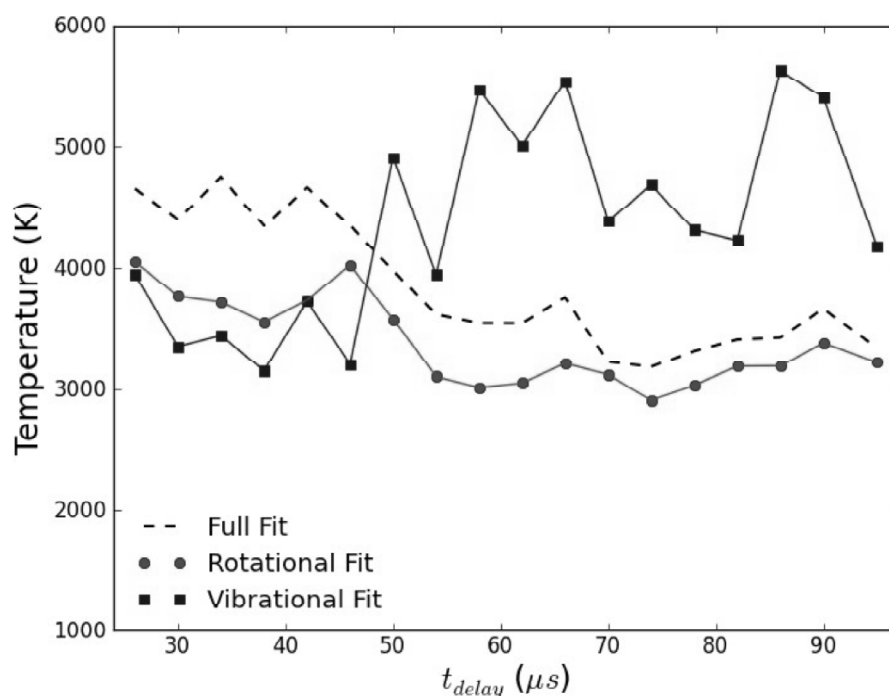
Figure 6: Inferred temperatures from Table 3 for the TiO $A^3\Phi \rightarrow X^3\Delta$ transition collected at various time delays

The implication of a local minimum as seen in the first set of our experimental runs is significant. Such a result is unexpected. Temperature is predicted to decrease with increasing time delay, as the laser-induced plasma equilibrates with the surrounding environment and cools. The presence of a local minimum with respect to temperature in regards to laser-induced plasma is sometimes indicative of combustion. In laser-induced plasma, combustion interrupts the overall cooling of the plasma and results in an increasing temperature for a brief time interval before the plasma ultimately resumes cooling. This process would thus result in a local minimum temperature followed by a local maximum with increasing time delay. Here, it is important to note that following certain laser pulses the induced plasma was observed to eject luminescent material resembling a flame.

The second set of measurements is meant to gain a clearer understanding of the expected transition temperatures for a given temporal region. The region of $t_{delay} = 26 - 36 \ \mu s$ was chosen on account of the local minimum observed in the first series of measurements. Provided that the observed increase in inferred temperature from the first measurements might be due to low signal to noise, this temporal region is expected to be especially bright without over powering the diatomic transitions of interest. The decrease in observation window of the 5 μs used for the first series of measurements to 2 μs is meant to temporally localize an inferred temperature. It was expected that each measurement would result in an inferred temperature slightly lower than the previous. The temperatures inferred by fitting each entire measured spectrum are consistent with each other and represent an overall decreasing temperature. However, the temperatures do fluctuate. These fluctuations are relatively small and are likely within the error associated with the temperature inferences.

In contrast to the unexpected temperature increase from the first set of measurements, the inferred temperature results by fitting the full measured spectra of third experimental run provide decreasing temperatures in this temporal region. For this series of measurements, a Ti sample which had not been previously ablated was used. The gate width of the collection window used is 2 μs. As with the second series of measurements, this gate width was chosen with the intent to more closely localize an inferred temperature with respect to time delay. When compared to the previous two runs, the third series of measurements covers a more expansive range of time delays.

The differences seen between the inferred temperatures for the first two experimental runs and the third series of measurements may be a result of the choice to replace the Ti sample. The Ti sample used for the third experimental

run had considerably less craters due to laser ablation than the sample used for the previous two series of measurements. Over the same temporal range covered in the first two experimental runs, the third series of inferred temperatures is on the order of 1000 K hotter. This is indicative of more electrons becoming free from the sample and contributing to the plasma. The results of the third experimental run are also void of the local minimum observed in the first. The rougher surface of the first experiment may have facilitated this phenomenon.

IV. DISCUSSION

While the results of the first experimental run seem to suggest chemical reactions in the ablation plume at the later time delays, such an explanation is not entirely convincing. For the later time delays of the second series of measurements, the TiO transitions became increasingly less prominent in the measured spectra. A low signal to noise ratio of the diatomic spectrum, when compared to other spectral contributions, will often contribute to inferred temperatures which are believed to be hotter than the actual temperature of the observed molecular transitions. This error is a consequence of poor signal to noise when using this particular method of inferring temperature, as the ratios of peak intensities of various transition lines are a key factor.

The results obtained by fitting only portions of the observed spectra believed to be dominated by rotational or vibrational transitions provide an intriguing element of analysis. It is predicted that the rotational transitions reach thermal equilibrium more readily than the vibrational transitions. Thus, distinguishing between a rotational and vibrational temperature could allow for a single spectrum collected at a given time delay to provide insight into which direction the temperature is trending. By inspecting Figure 4, the inferred vibrational temperatures provide a parabolic shape similar to that of the inferred rotational temperatures, only delayed. Figure 5 provides an image of the inferred vibrational temperature decreasing to that of the rotational temperature. Recall, the second experimental run gathered measurements near the local minimum provided by the inferred temperatures of the first series of measurements. Figure 6, however, does not portray this predictive behavior for the inferred rotational temperatures. While the inferred temperature from the full spectrum fit and the inferred rotational temperature are consistent with one another, the inferred vibrational temperature for the third experimental run is unreliable.

The error associated with an inferred temperature by fitting a measured spectrum with computed diatomic molecular spectra by use of a Nelder-Mead algorithm is typically no greater than 10%. Such error predictions are determined by use of Monte Carlo type simulations varying the spectral background of a measurement. The background adjusted spectra are then used to infer a temperature. This process is sufficiently repeated creating a range of temperatures for statistical analysis. Since the peak to peak ratios of the observed spectral transitions factor into the determination of a temperature, this type of background variation is analogous to inferences made from shot-to-shot LIBS measurements.

The current research presented in this work is intended to gain an understanding of the temporal evolution of TiO in laser-induced plasma. However, a comprehensive understanding of such requires spatial resolution, as well. The plasma plume produced for each laser event appeared consistent to its predecessor, and a similar region of the plume was imaged onto the slit of the spectrometer for each event. However, measurements such as these provide a glimpse into only this arbitrary region of the plasma. The temporal behavior of TiO is not expected to be localized to one such specified region. It is likely that TiO evolves in time along the height and depth of the laser-induced plasma plume. This sort of analysis will be the topic of future investigations concerning temperature inference in laser-induced plasma.

References

[1] A. Christy, *Phys. Rev.* **33**, 701-730, (1929).

[2] D. Kotnik-Karuza, R. Jurdana-Šepić, *Astron. Astrophys.* **355**, 595-602, (2000).

[3] K. C. Namiki, H. Saitoh, H. Ito, *J. Mol. Spectrosc.* **226**, 87-94, (2004).

[4] S. J. Schmidt, G. Wallerstein, V. Woolf, J. L. Bean, AIP 978-0-7354-0627-8, (2009).

[5] E. L. Martín, X. Delfrosse, G. Basri, B. Goldman, T. Forveille, M. R. Z. Osorio, *Astrophys. J.* **118** 2466-2482, (1999).

[6] K. Lodders, *Astrophys. J.* **577**, 974-985, (2002).

[7] B. M. Krupp, J. G. Collins, and H. R. Johnson, *Astro. Phy. J.* **219**, 963-969, (1978).

[8] U. G. Jørgensen, *Astron. Astrophys.* **284**, 179-186, (1994).

[9] J. G. Collins and T. D. Faÿ, Jr., *J. Quant. Spectrosc. Radiat. Transfer* **14**, 1259-1272, (1974).

[10] D. W. Schwenke, *Faraday Discuss.* **109**, 321-334, (1998).

[11] F. Allard, P. H. Hauschildt, and D. Schwenke, *Astro. Phy. J.* **540**, 1005-1015, (2000).

[12] L. Linsebigler, G. Lu, J. T. Jr. Yates, *Chem. Rev.*, **95**, 735-758, (1995).

[13] D. F. Ollis, CR Acad. Sci. Ser. IIC **3** (6), 405-411, (2000).

[14] B. O'Regan and M. Grätzel, *Nature* **353**, 737, (1991).

[15] C. D. Grant, A. M. Schwartzberg, G. P. Smestad, J. Kowalik, L. M. Tolbert, J. Z. Zhang, *J. Electroanal. Chem.* **522**, (1), 40-48, (2002).

[16] J. Hermann, A. Peronne, C. Dutouquet, *J. Phys. B: At. Mol. Opt. Phys.* **34**, 153-164, (2001).

[17] C. G. Parigger, A. C. Woods, A. Keszler, L. Nemes, J. O. Hornkohl, AIP Conf. Proc. 1464, 628-640 (2012); doi: 10.1063/1.4739915.

[18] A. C. Woods, C. G. Parigger, J. O. Hornkohl, *Opt. Lett.* **37**, 5139-5141, (2012).

[19] A.C. Woods, C.G. Parigger, A. Keszler, L. Nemes, and J. O. Hornkohl, *Int. Rev. Atom. Mol. Phys.* **3**, 51-59, (2012).